AIAA 2004–1758

Design of a Low-Boom Supersonic Business Jet Using Evolutionary Algorithms and an Adaptive Unstructured Mesh Method

Seongim Choi and Juan J. Alonso
Stanford University, Stanford, CA 94305-3030

Hyoung S. Chung
Korean Air Force Academy, Korea

45th AIAA/ASME/ASCE/AHS/ASC Structures, Structural Dynamics and Materials Conference
April 19–22, 2004/Palm Springs, CA

AIAA 2004–1758

Design of a Low-Boom Supersonic Business Jet Using Evolutionary Algorithms and an Adaptive Unstructured Mesh Method

Seongim Choi* and Juan J. Alonso†
Stanford University, Stanford, CA 94305-3030

Hyoung S. Chung‡
Korean Air Force Academy, Korea

The purpose of this study is to establish the feasibility of using constrained, multi-objective, evolutionary algorithms for the design of supersonic, low-boom aircraft in combination with high-fidelity modeling of the external aerodynamic flow. The objective functions that we attempt to minimize simultaneously are the aircraft coefficient of drag at a fixed lift coefficient, and two different measures of the noise level generated by the sonic boom signature at the ground. As part of this work we have developed an analysis tool, BOOM-UA, which fully automates the process of CAD geometry and mesh generation, solution adaptation, and signature extraction and propagation. BOOM-UA is based on the AirplanePlus unstructured tetrahedral solver for the Euler and Navier-Stokes equations. In previous work we have conducted a careful study regarding the number of solution adaptive refinement levels and mesh density that are required to accurately predict the sonic boom signature at the ground. Since the cost of driving BOOM-UA directly for reasonable design problems (> 20 design variables) with even the most efficient GAs is beyond the capabilities of modern day supercomputers, Kriging approximation models were constructed from a database of CFD analyses and used in conjunction with the GAs in order to minimize the cost of the computation. This procedure is able to generate a set of Pareto-optimal solutions for the sonic boom and drag objectives that are also forced to satisfy the specified constraints. Optimized shapes for both minimum initial pressure jump, Δp, and preceived noise level, PNdB, are discussed and their boom signatures are compared. The result of this effort shows that the current generation of computer clusters is able to treat significant design problems (between 20 and 50 design variables) with reasonable accuracy, cost, and turnaround time.

INTRODUCTION

SONIC booms have been the main reason preventing supersonic flight over inhabited areas. The minimization of the environmental impact from this kind of aircraft is one of the fundamental issues to be resolved since studies have shown that such aircraft would have great market potential should they be allowed to fly supersonically over land.[1,2] For these reasons, research efforts have been recently focused on various techniques for sonic boom mitigation[4,6–8,18] and non-linear CFD has emerged as an essential tool owing to the increasing availability of large computing resources.

The nature of this problem is more complicated than the traditional Aerodynamic Shape Optimization problem (ASO): not only must we deal with multiple objectives simultaneously (boom and performance) but the design space for the sonic boom objective has been shown to exhibit multiple local minima, and to be rather noisy and even discontinuous.[5] These characteristics of the design problem rule out the possibility of using gradient-based optimization (and the powerful adjoint method[9,11–13]) for the boom portion of the problem. Moreover, the computational cost is exacerbated by the fact that an accurate pressure distribution must be computed a certain distance beneath the aircraft (not *on* the aircraft surface as it is normally the case for ASO) and therefore an extremely fine mesh is required for the computations. Finally, the details of the geometry and the relative arrangement (distributions of volume and lift) of the components of the configuration are very important for accurate sonic boom predictions and, therefore, if the procedure is to be automated, it becomes important to have automatic, high-quality, geometry generation, and the ability to create complex meshes without user intervention. The combination of all of these requirements has lead us to the use of GAs combined with unstructured adaptive meshing technologies.

*Doctoral Candidate, AIAA Member
†Assistant Professor, AIAA Member
‡Assistant Professor, AIAA Member

However, before sonic boom minimization work can be credibly carried out, the accurate prediction of the fundamental sonic boom propagation problem has to be validated. In our previous work,[3] numerical and mesh resolution requirements for accurate sonic boom computations were established for both the computation of near-field pressures and ground boom signatures. Results were verified with wind-tunnel experiments using the inviscid version of our solver and good agreement was found for relatively fine (on the order of 5-7 million nodes) solution-adaptive meshes.

Once the solution requirements for accurate sonic boom computation have been determined, the design of supersonic configurations can proceed. In our early design efforts,[4,6] we had only considered two main objective functions in an *unconstrained* multi-objective design formulation: the drag coefficient of the aircraft at a fixed lift coefficient, and the magnitude of the initial peak of its ground boom signature. In this work, additional constraints that guarantee a feasible aircraft with the required range and suitable trim and stability behavior are specified. In order to highlight the differences in the results when using two different noise measures, we include a comparison between the shapes that result from using the initial pressure rise and the perceived loudness as part of our multi-objective optimization.

Our design procedure, as will be explained later, relies on the ability to compute a large number of geometrically-complex solutions for different values of the design variables in a short amount of time. Our analyses are carried out using a fully nonlinear, three-dimensional environment built from a number of independent modules including an unstructured adaptive flow solver,[19] the Centaur unstructured mesh generation/adaption system,[32] the AEROSURF CAD-based geometry kernel,[17] and the ground boom prediction software PCBoom3.[31] The execution of all these modules has been fully automated into a single analysis tool which we call BOOM-UA.

But MDO methods, particularly those based on high-fidelity analyses, greatly increase the computational burden and complexity of the design process[33,34,36,37] even with fully parallelized modules based on domain decomposition schemes. For this reason, high-fidelity analyses typically used in single discipline designs may not be suitable for direct use in MDO.[33,35] In fact, even in single discipline designs, the cost of high-fidelity models may become prohibitive, particularly in combination with Genetic Algorithms for the optimization. Faced with these problems, the alternative of using approximation models of the actual analyses has received increasing attention in recent years.

The Kriging technique, developed in the field of geostatistics, has been recognized as an interesting choice for approximation models of computationally expensive CFD analyses. In theory, it is able to interpolate sample data and to model functions with multiple local extrema.[27,38] Using variations of the method of design of experiments (DOE), the Kriging model can efficiently represent global trends in the design space. The basis functions chosen for the underlying Kriging approximation determine, to a large extent, the quality of the approximation.

Once an accurate approximation model is generated (at a computational cost that increases with the number of design variables in the problem and the breadth of the design space), it can be used to search for optimum combinations of the design variables within the design space. Since the Kriging model can represent multi-modal functions with relatively low computational cost it is a good candidate for use with global optimizers such as genetic algorithms for the solution of the low-boom problem.

Our design procedure is then based on the following key ingredients:

- An automatic tool for the computation of flow fields and sonic boom signatures, BOOM-UA.
- The construction of Kriging approximation models of the responses (aerodynamic performance and sonic boom loudness.)
- A non-dominated sorting genetic algorithm.
- The application of constraints to limit the infeasibility of the resulting designs.

It is worth mentioning that, when it comes to multi-objective optimization problems, there is not a single best solution but rather a non-dominated solution set must be obtained (the so-called Pareto set.) In our work, the Non-dominated Sorting Genetic Algorithm II (NSGA II) of Srinivas and Deb[39] is used.

The procedure is straightforward. First, a large number of sample points in the design space (at which CFD solutions will be computed using BOOM-UA) are generated using the Latin Hypercube Sampling technique. Then, Kriging approximation models are constructed (based on this initial population) for the drag coefficient, the initial shock strength, and the perceived noise level. Using these approximation models and two simple constraints related to trim, longitudinal stability and mission performance, a GA-based optimization is performed to produce an expected Pareto set. The points on the approximation-model-based Pareto set are evaluated using BOOM-UA and the differences between the predicted and actual values can be used to shrink or enlarge the size of a trust region. This procedure can be repeated iteratively until the predicted and computed Pareto sets converge to each other (the procedure can be stopped earlier if the differences are sufficiently small.) We have carried out

such a procedure and the results are detailed in the following sections.

The results show that the minimization of the loudness of the ground sonic boom with constraints is more difficult to achieve compared to unconstrained optimizations where configuration parameters such as the sweep angle are allowed to attain unreasonable values. The amount of reduction in the boom figure of merit is not as large as for unconstrained optimization.

AERODYNAMIC ANALYSIS : BOOM-UA

All of the necessary modules to carry out aerodynamic analyses and ground boom signature computations are integrated into our analysis tool, BOOM-UA. The complete procedure is fully automated for efficiency and for the ability to include BOOM-UA in a design loop. Firstly, a parameterized geometry is represented directly with a CAD package (ProEngineer in this study) using a collection of surface patches. A baseline unstructured tetrahedral mesh is generated by the user with the Centaur software. Our geometry kernel, AEROSURF generates variations of the baseline configuration. If the changes in the geometry are small enough we can perturb the baseline mesh to conform to the deformed shape without problems with decreased mesh quality and/or edge crossings. Otherwise, an automatic mesh regeneration procedure has been implemented to accommodate large changes in the geometry. Our inviscid Euler solver, AirplanePlus calculates the surface pressure distributions and predicts both C_L and C_D and the near-field pressures which can then be propagated to the ground to obtain ground boom signatures. A solution-adaptive mesh refinement procedure is interfaced with the flow solver to generate refined meshes adapted according to a criterion based on the pressure gradient information obtained by the flow solver. The boom prediction software PCBoom3 is used for the propagation portion of the solution procedure. Three-dimensional near-field pressure distributions are extracted on a cylindrical surface several body lengths beneath the configuration and are provided to the boom propagation tool. Figure 1 shows a brief schematic of all the processes that have been integrated into BOOM-UA. In this Figure, n refers to the number of design points. Each individual module is explained in detail in the following subsections.

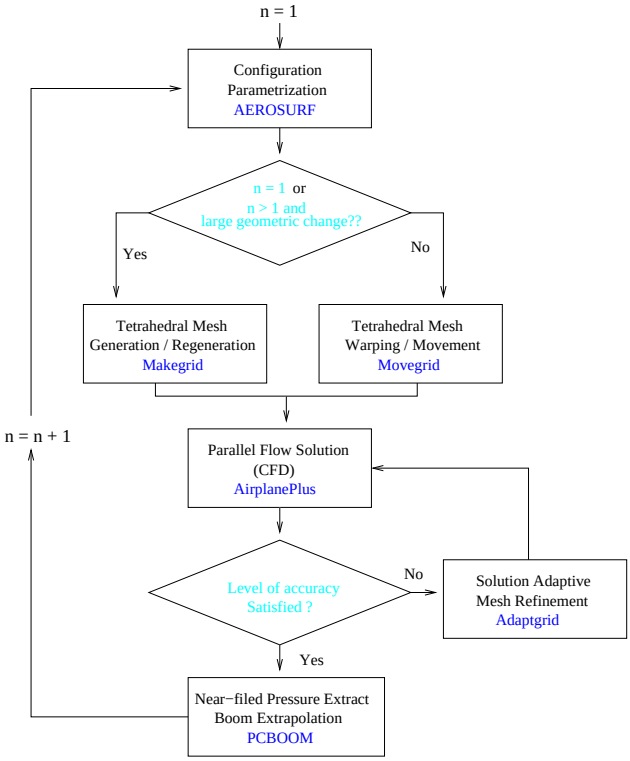

Fig. 1 Schematic of aerodynamic analysis tool, BOOM-UA

CAD Geometry Representation

High-fidelity MDO requires a consistent high-fidelity geometry representation. In general, the geometric shape of an aircraft can be defined by an appropriate parameterization of the geometry. This parametric geometry kernel is available to all of the participating disciplines in the design so that both cost functions and constraints can be computed using the same geometry representation.

In our work, a CAD-based geometry kernel is used to provide this underlying geometry representation. Baseline shapes are developed in a CAD-package (ProE, in our case) and constitute our parametric master model; they uniquely define the parameterization of a configuration given a particular design intent.

Our geometry kernel (AEROSURF) is coupled with the parametric CAD description through the CAPRI interface of Haimes,[14,17] such that it automatically generates watertight surface geometry patches. AEROSURF can be executed in parallel and uses a distributed geometry server to expedite the generation of a large number of different design alternatives, thus reducing the cost of running geometry regenerations in the CAD package. Using a master/slave approach and PVM for distributed computing, arbitrary numbers of slaves can be started simultaneously while a master program maintains a queue of geometry regeneration requests and keeps slaves busy doing CAD re-generations.

Furthermore, AEROSURF has the capability of generating automatic surface meshes (both triangular and patched-quadrilateral) that can be linked directly with the volume mesh generation portion of Centaur. This surface geometry generation tool can effectively be incorporated into our unstructured mesh generation environment for the automatic treatment of complex configurations, including the presence of nacelles, diverters, etc. Figure 2 shows a baseline geometry with

46 surface patches and 108 design variables, which is generated directly in ProEngineer.

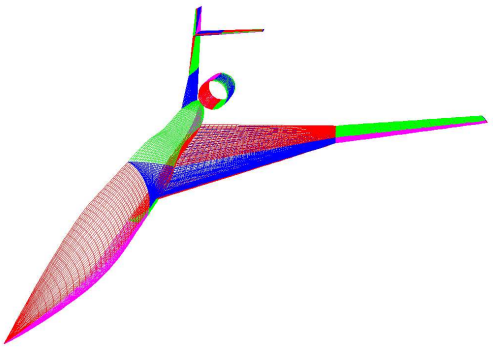

Fig. 2 Geometry representation by parametric, CAD-interfaced AEROSURF

Tetrahedral Unstructured Mesh and Solution Approach

In this work we focus on the use of unstructured tetrahedral meshes for the solution of the Euler equations around complete aircraft configurations. The most popular methods of generating unstructured meshes[20–22] are the advancing-front and Delaunay triangulation methods. In this work, the advancing-front method is chosen and the Centaur grid generation software[32] is used. The advancing-front method[23] involves the simultaneous generation of mesh points and their connectivity. The main process reduces to building the mesh iteratively element by element, adding new elements to previously generated elements, thus sweeping out a front across the entire domain. This method usually relies on an explicitly defined element-size distribution function, which is most often constructed using a background octree grid[23,24] for size and stretching information and plays a major role in the success of this method.

One of the advantages of the advancing front method, like any other marching method, is its restarting capability. Since the only data required to restart the generation process are given by the current front, information regarding the already generated grid behind the current front is not necessary. Also boundary integrity is guaranteed since this process starts from a discretization of the solid boundaries.

The Centaur software is directly linked with the surface representation obtained from AEROSURF, and is used to construct meshes for aircraft configurations and to enhance grid quality through automatic post-processing. Only fine meshes need to be explicitly constructed since our multigrid algorithm is based on the concept of agglomeration and, therefore, coarser meshes are obtained automatically. The following Figure 3 shows a triangular mesh on the body surface and the symmetry plane of our configuration. For visualization purposes only, a coarsened grid is shown.

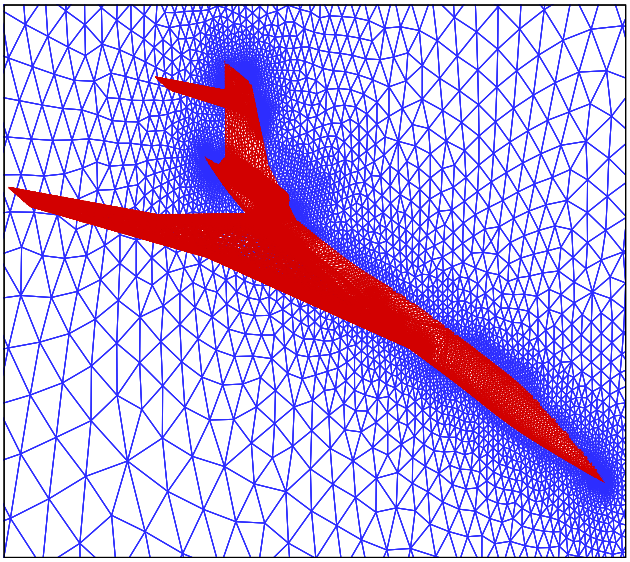

Fig. 3 Unstructured tetrahedral surface mesh around a low-boom aircraft

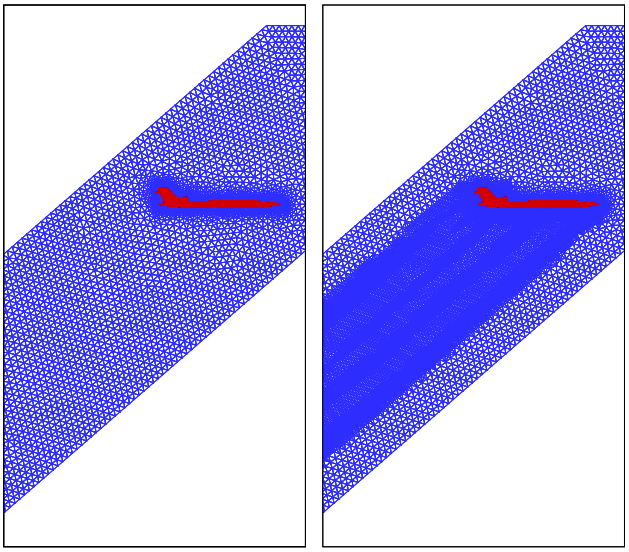

Fig. 4 Mesh before and after two adaption cycles

The three-dimensional, unstructured, tetrahedral AirplanePlus inviscid flow solver is used in this work. AirplanePlus is a C++ implementation of the original AIRPLANE flow solver of Jameson[25] by Van der Weide with substantial enhancements to the baseline algorithm. An agglomeration multigrid strategy is used to speed up convergence. A modified Runge-Kutta time stepping procedure with appropriately tailored coefficients is used to allow for high CFL numbers. Several options for artificial dissipation and the block-Jacobi preconditioning method are all available in the solver. Figure 5 shows a pressure plot on the surface of our baseline configuration flying at $M_\infty = 1.5$ and at $C_L = 0.1$. Figure 6 shows the pressure on the symmetry plane for the same configuration showing

the propagation of all shock waves at the same flow conditions.

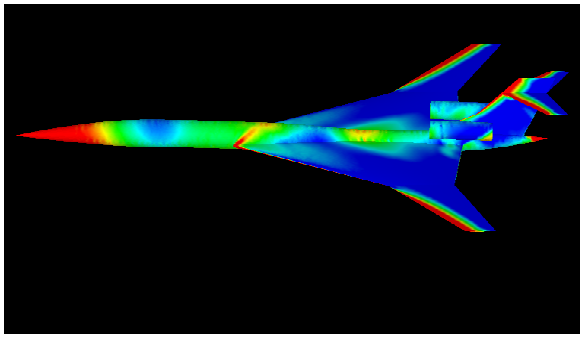

Fig. 5 Pressure plot around aircraft surface, M=1.5

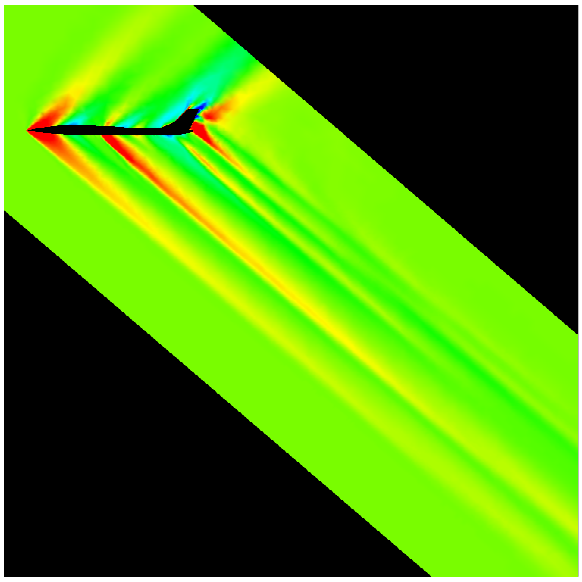

Fig. 6 Pressure plot on the symmetry plane, M=1.5

Solution Adaptive Refinement

Once an initial solution has been computed on the tetrahedral mesh, the grid needs to be locally refined to better capture specific features with higher accuracy at lower cost. For the cases of steady-state flows that we are investigating, coarsening has only a minor performance impact and is omitted in this work, although the mesh generation system is capable of automatically coarsening meshes in areas that do not require the resolution provided.

An element subdivision (h-refinement) method is employed. This is implemented with strict hierarchical subdivision rules[15] to prevent degradation of grid quality at each subsequent adaption phase. For each edge that is flagged for refinement by the solution-based error estimation criteria, a new node is inserted at its midpoint and reconnected to form new tetrahedral children. Highly anisotropic children may not be refined further to ensure high grid quality.

For cells with hanging nodes resulting from the interface of refined and non-refined regions and for anisotropic cells requiring further refinement, the children cells are removed and their parent cells are isotropically refined to ensure a compatible refinement pattern.

Finally, for boundary edges, these newly inserted nodes are repositioned onto the splined surface which defines the original surface from the CAD package. Also, undesirable shape measures are investigated and new local tetrahedral configurations with more desirable shape measures are selected.

All of these refinement procedures are included in the Centaur mesh generation package that we use for this work.

Another important issue in solution adaptive refinement for complex problems is the choice of an appropriate error indicator. Most widely-used refinement options to estimate errors or detect flow features are gradient-based criteria driven by the physical flow variables. Gradients of pressure can be used to identify inviscid flow features. But in sonic boom prediction problems, the pressure gradient in the near-field (which has a much lower magnitude) is just as important as in the neighborhood of the aircraft.

In this case, the refinement criterion is not simply based on the gradient of the pressure because the strongest shocks in the neighborhood of the aircraft will then be the only target of refinement, leaving weaker shocks in near field unresolved.

A solution-adaptive refinement procedure with a constraint on the cell size inside a specific region of interest, which can be predicted from a straightforward shock angle calculation, is best suited to the sonic boom prediction problem.

A reasonable predictor of the shock location can be based on the magnitude of the local velocity vector projected onto the direction of the local pressure gradient. A mathematical expression for this refinement criterion is presented below. In the expression for the adaption criterion, $\mathbf{V}$ is the velocity vector, c is the speed of sound and $\triangle x$ is the required minimum edge length which is often problem dependent.

$$\epsilon' = \frac{\mathbf{V}}{c} \cdot \frac{\nabla p}{|\nabla p|} \tag{1}$$

Numerical experiments[16] indicate that a modification of the previous equation to include a mesh length-scale such as:

$$\epsilon = \frac{\mathbf{V}}{c} \cdot \frac{\nabla p}{|\nabla p|} \triangle x \tag{2}$$

produces a more effective refinement criterion for shock/expansion flows by increasing the control over the size of triangles. The adaption procedure is repeated until a specified accuracy is achieved or a maximum number of refinement levels has been reached.

Figure 4 shows two meshes. The first one is the original mesh (number of nodes = 562,057) before adaption and the second one shows the solution-adapted mesh (number of nodes = 1,028,577) after two adaption steps. Typically three or four consecutive adaption cycles are performed automatically starting from the initial mesh to reach the necessary mesh resolution. The necessary mesh resolution for all designs in this work is determined by the results of a previous study.[3]

Ground Boom Propagation

The basic strategy for the computation of ground boom signatures can be seen in Figure 7 below. A solution adaptive mesh using the criteria described above is constructed around the aircraft. It extends a certain distance away from it, but not to the ground plane as it would be computationally prohibitive to do so with appropriate resolution from the cruise altitude. At the near-field plane location, the pressure signature created by the aircraft is extracted and it is propagated down to the ground using extrapolation methods based on geometric acoustics.

The far-field boundaries of the CFD mesh must be located close enough so that the resulting mesh size is computationally manageable, but, at the same time, they must be located far enough so that the near-field flow field is axisymmetric and there are no remaining diffraction effects which cannot be handled by the extrapolation scheme.

In this work, the pressure field on the symmetry plane 1.2 body lengths below the aircraft is obtained and provided as an initial condition to the boom extrapolation program. The pressure extraction algorithm (for the unstructured tetrahedral mesh) is based on advanced octree data structures and therefore incurs very little computational cost.

In this work, we are using both the Sboom[30] and PCBoom3[31] extrapolation methods to propagate near-field signatures into ground booms. Although the PCBoom3 software is far more capable than Sboom, we have only computed ground booms created by the aircraft in a steady-state cruise condition and, therefore, both codes are nearly equivalent. If ground booms caused by maneuvering aircraft were to be computed, the capabilities of the PCBoom3 software would have to be used.

The two sonic boom extrapolation methods account for vertical gradients of atmospheric properties and for stratified winds (the winds have been set to zero in this work.) Both methods essentially rely on results from geometric acoustics for the evolution of the wave amplitude, and both utilize isentropic wave theory to account for nonlinear waveform distortion due to atmospheric density gradients and stratified winds.

There are additional extrapolation/propagation methods that are based on the concept of an F-function[29] but these have not been used in this work as they assume no variation of the near-field signature in the azimuthal direction, which is normally not the case in our computations.

In three-dimensional wave propagation cases, the pressure data on a cylindrical surface centered along the aircraft longitudinal axis is extracted instead and propagated along rays in directions that are not necessarily perpendicular to the ground. The propagation scheme marches these *rays* down to the ground from all azimuthal directions that may eventually reach the ground. Depending on the atmospheric conditions and flight altitude, a cutoff angle will exist beyond which no disturbance will reach the ground: refraction effects divert the noise propagation back toward the upper atmosphere.

Our earlier research on low-boom aircraft design was mainly focused on the reduction of the magnitude of only the initial peak of the ground boom signature.[18] This requirement, which had been suggested as the goal of the DARPA-sponsored Quiet Supersonic Platform (QSP) program ($\Delta p_0 < 0.3$ psf), hides the importance of the rest of the signature, which often arises from the more geometrically complex aft portion of the aircraft where empennage and engine nacelles and diverters create more complicated flow patterns. Moreover, such designs often have two shock waves very closely following each other in the front portion of the signature,[5,7] a behavior that is not robust and is therefore undesirable.

For this reason, we have chosen to base our designs on the perceived loudness of the complete signature as well as the initial peak of ground boom. Frequency weighting methods are used due to the unique property of the human hearing system which doesn't have an equal response to sounds of different frequencies. In these calculations, less weighting is given to the frequencies to which the ear is less sensitive.

VALIDATION OF BOOM-UA

The accuracy of our aerodynamic analysis tool, BOOM-UA, has been validated in previous work[3] to guarantee that the results of our optimizations can be trusted. Experimental near-field pressure data were available from a NASA Langley wind-tunnel test.[10] The model consists of a wing with a large outboard dihedral/winglet, fuselage, vertical tail, and aft-fuselage mounted nacelles with diverters attached to the fuselage. To determine which changes correspond to increasing geometric complexity, two additional configurations were also tested. To obtain these two additional configurations, the nacelles and diverters are first removed and, then, both the tail and nacelles/diverters are omitted.

BOOM-UA was applied to all three configurations to extract the near-field overpressures and to predict the ground boom signatures. The near-field overpressures were extracted at three distances from the air-

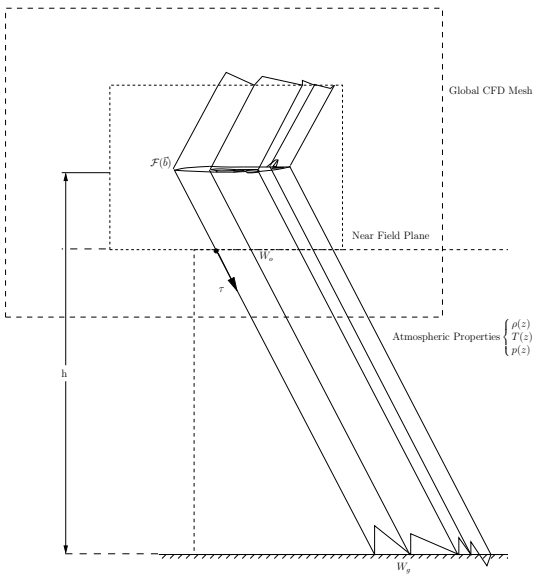

Fig. 7 Schematic of sonic boom propagation procedure.

craft model (9.5 in, 12 in, and 16 in) corresponding to the locations where experimental data was taken. This allows us to compare the CFD predictions directly with experiment and to compute ground signatures extrapolated from these distances.

Our mesh resolution study required up to 4 adaption cycles (the finest meshes had about 8 million nodes obtained by solution-adaptively refining an initial mesh with only 0.5 million nodes) to predict accurately the near-field pressure distributions given in the experiments. The results from the finest mesh show very good agreement with the experiment both in the near-field pressures and ground boom signatures. Figure 8 shows the comparison of the near-field pressure at 9.5 in below the complete configuration with nacelles and tails, and figure 9 corresponds to 12 in below the same configuration. Ground boom signatures propagated from those locations were also computed using BOOM-UA and compared with experimental data. Figures 10 and 11 show good agreement between the computations and experiments for the ground boom signatures.

Now that the accuracy of our aerodynamic analysis tool, BOOM-UA, has been validated, the optimization procedure can be reliably combined with the approximation model which is generated by BOOM-UA.

MULTI-OBJECTIVE OPTIMIZATION

The minimization of the loudness of the ground boom normally comes at the expense of the performance of other disciplines participating in the design. For example, most shape changes that will improve the sonic boom of an aircraft will have a detrimental effect on the cruise drag coefficient. The converse

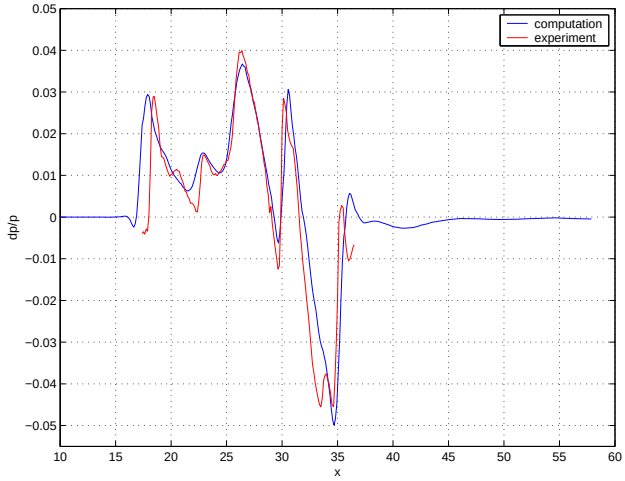

Fig. 8 Comparison of near-field pressure 9.5 in below the configuration

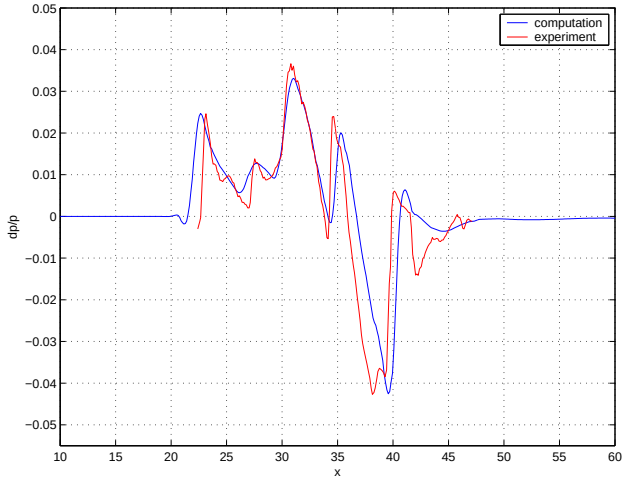

Fig. 9 Comparison of near-field pressure 12 in below the configuration

also tends to be true: changes to the shape that result in improvements in aerodynamic performance tend to worsen the sonic boom characteristics.

For the low-boom problem, obtaining a solution which simultaneously optimizes all the objectives is not possible and the concept of the optimal Pareto set becomes important, as it suggests a set of solutions which are superior to the rest with respect to all objective criteria, but are inferior to other solutions in one or more of the objectives. Once the set of optimal solutions has been identified, it is up to the designer to choose the one solution, out of many possible ones, that best meets the overall purpose of the design. A genetic algorithm can use this dominance criteria in a straightforward fashion to drive the search process toward the Pareto front.

Due to the unique features of GAs, which work with a population of solutions, multiple Pareto optimal solutions can be captured in a single optimization run. This is the primary reason that makes GAs ide-

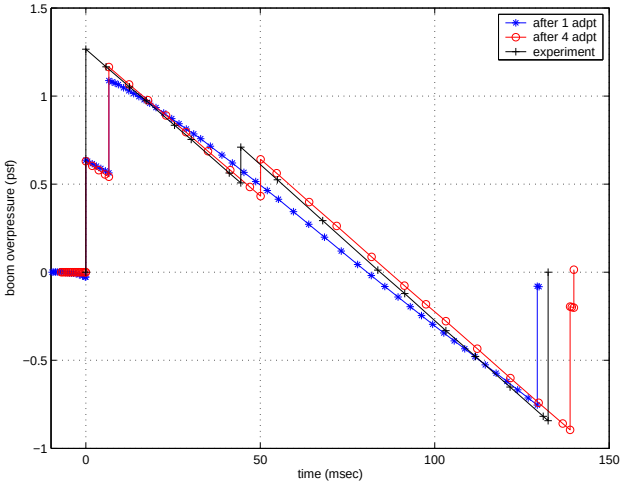

Fig. 10 Comparison of ground boom extrapolated from 9.5 in below the configuration

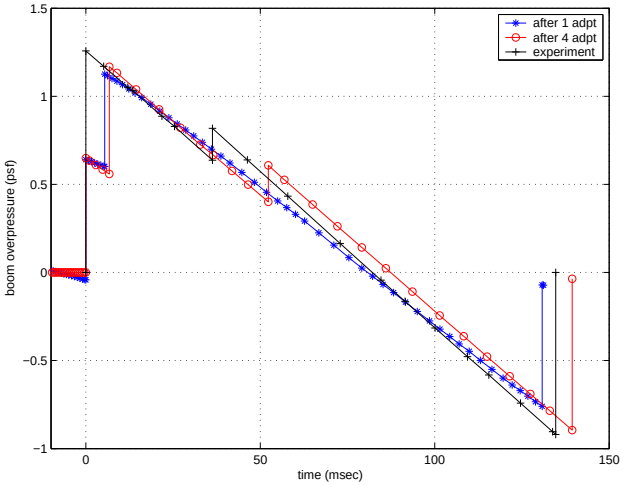

Fig. 11 Comparison of ground boom extrapolated from 12 in below the configuration

ally suited for multi-objective optimization. However many of the existing MOEAs have been criticized for their computational complexity (which is related to the ranking/sorting of the individuals in a generation by comparison of their fitness) and for the need to specify a sharing parameters. The Non-dominated Sorting Genetic Algorithm (NSGA-II) was used to alleviate these problems and has shown to have fast convergence rates.

However, the direct combination of CFD analysis with GAs can be very expensive due to the high computational cost for the evaluation of the fitness of each member of the population and the large number of generations required to reach the Pareto front: often GAs require large populations and many generations to locate the global extremum of complex design spaces. If a fairly accurate global approximation model for the CFD analysis can be constructed, its combination with GAs can be tractable. A Kriging approximation model has been used successfully in combination with GAs.[4]

In this study, Kriging approximation models are constructed from a large number of members of an initial population using the results from repeated analyses carried out with BOOM-UA. The approximation model is combined with the NSGA-II algorithm to minimize ground boom intensity while maintaining acceptable levels of aerodynamic cruise performance.

Kriging Approximation Model

The Kriging approximation technique, developed in the field of spatial statistics, has been drawing attention as an alternative to expensive CFD simulations. This interpolation technique creates a surface fit from measured sample data using advanced statistical methods. While searching for data trends and global and local outliers, the ability of the Kriging method to capture multiple local extrema is fundamental in global optimization.

The Kriging technique uses a two-component model that can be expressed mathematically as

$$y(\boldsymbol{x}) = f(\boldsymbol{x}) + Z(\boldsymbol{x}) \tag{3}$$

where $f(\boldsymbol{x})$ represents a global model and $Z(\boldsymbol{x})$ is the realization of a stationary Gaussian random function that creates a localized deviation from the global model.[26] If $f(x)$ is taken to be an underlying constant,[27] β , Equation (1) becomes

$$y(\boldsymbol{x}) = \beta + Z(\boldsymbol{x}), \tag{4}$$

which is used in this paper. The estimated model of Equation (2) is given as

$$\hat{y} = \hat{\beta} + \boldsymbol{r}^T(\boldsymbol{x})\boldsymbol{R}^{-1}(\boldsymbol{y} - \boldsymbol{f}\hat{\beta}), \tag{5}$$

where $\boldsymbol{y}$ is the column vector of response data and $\boldsymbol{f}$ is a column vector of length n_s which is filled with ones. $\boldsymbol{R}$ in Equation (3) is the correlation matrix which can be obtained by computing $R(\boldsymbol{x}^i, \boldsymbol{x}^j)$, the correlation function between any two sampled data points. This correlation function is specified by the user. In this work, we use a Gaussian exponential correlation function of the form provided by Giunta, et al.[28]

$$R(\boldsymbol{x}^i, \boldsymbol{x}^j) = \exp\left[-\sum_{k=1}^{n} \theta_k |\boldsymbol{x}_k^i - \boldsymbol{x}_k^j|^2\right]. \tag{6}$$

The correlation vector between $\boldsymbol{x}$ and the sampled data points is expressed as

$$\boldsymbol{r}^T(\boldsymbol{x}) = [R(\boldsymbol{x}, \boldsymbol{x}^1), R(\boldsymbol{x}, \boldsymbol{x}^2), ..., R(\boldsymbol{x}, \boldsymbol{x}^n)]^T. \tag{7}$$

The value for $\hat{\beta}$ is estimated using the generalized least squares method as

$$\hat{\beta} = (\boldsymbol{f}^T\boldsymbol{R}^{-1}\boldsymbol{f})^{-1}\boldsymbol{f}^T\boldsymbol{R}^{-1}\boldsymbol{y}. \tag{8}$$

Since $\boldsymbol{R}$ is a function of the unknown variable $\boldsymbol{\theta}$, $\hat{\beta}$ is also a function of $\boldsymbol{\theta}$. Once $\boldsymbol{\theta}$ is obtained, Equation

(3) is completely defined. The value of $\boldsymbol{\theta}$ is obtained by maximizing the following function over the interval $\boldsymbol{\theta} > \mathbf{0}$

$$-\frac{[n_s \ln(\hat{\sigma}^2) + \ln|\boldsymbol{R}|]}{2}, \tag{9}$$

where

$$\hat{\sigma}^2 = \frac{(\boldsymbol{y} - \boldsymbol{f}\hat{\beta})^T \boldsymbol{R}^{-1} (\boldsymbol{y} - \boldsymbol{f}\hat{\beta})}{n_s}. \tag{10}$$

In order to construct a Kriging approximation the only data required are the function values at a number of pre-specified sample locations. For many computational methods, secondary information such as gradient values may be available as a result of the analysis procedure and can be used to enhance the accuracy and to lower the cost of the Kriging approximation.[4]

Non-dominated Sorting Genetic Algorithms

When several criteria are considered in an optimization problem, the optimal solution is generally not unique since no point can be considered *best* with respect to all criteria simultaneously. Instead, optimal solutions on the Pareto set, which contains all non-dominated solutions, can be identified. Genetic Algorithms (GAs) simultaneously operate on a population of potential solutions and build a database of solutions which can be thought of as a cloud of points in solution space. At convergence, the cloud ceases to evolve and its convex hull determines the optimal Pareto set. Our results in multi-objective optimization are based on the algorithm of Srinivas and Deb: the Non-dominated Sorting Genetic Algorithm (NSGA).[39]

First, this algorithm applies non-dominance definitions to each individual in a population according to their fitness value. But, in a multi-objective optimization problem, different fitness values are assigned to each candidate design corresponding to the various design criteria. Therefore, to evaluate the individuals, a ranking is necessary and the candidate designs are classified by fronts. The non-dominated sorting procedure requires a ranking selection method which emphasizes the optimal points. Therefore, the sharing technique, or niche method, is used to stabilize the subpopulations of the 'good' points.

The main concern related to the use of GAs in optimum designs is the computational effort needed. In difficult problems, GAs require bigger populations and this translates directly into higher computational effort for the optimization algorithm itself. In the case of our multi-objective problem, two objectives along with several constraints should be evaluated for each individual, which means that the computational effort is rather large. One of the main advantages of GAs is that they can be easily be parallelized.[40] At each generation, the fitness values associated with each individual can be evaluated in parallel. In this study, we have only two fitness functions at a time along with a small number of constraints and the parallelization of NSGA-II is not necessary. However for future problems involving a large number of objective functions with the consideration of several constraints, a parallelized NSGA-II can be effectively used.

TEST PROBLEMS AND RESULTS

Design Problems

A baseline configuration for the first design cycle is chosen from the result of an aero-structural design carried out in our previous work.[17] This configuration has been optimized for minimum drag with no attention paid to sonic boom. By choosing an initial baseline which was already optimized for drag we can investigate the effect of adding a second objective (such as reducing sonic boom.)

First, seventeen design variables are chosen to allow reasonable geometric changes from the initial baseline configuration. The values of these design variables are chosen using a random Latin Hypercube sampling technique in order to generate parametric CAD definitions of the geometry for each of the initial members of a population. In this study 232 initial sample design points were selected to accommodate possibly large variations in the design space corresponding to rather large geometric changes. Variations as large as 30% for each of the seventeen design variables are used in the first cycle of this study.

Most of the geometric changes are restricted to the wing and fuselage. Fuselage camber and radii at five sections which are equally spaced along the fuselage length can be changed, while the location and shape of the wing are also varied. The wing reference area is also allowed to vary, although the reference area for the initial baseline is used to calculate aerodynamic coefficients such as C_L and C_D.

The seventeen design variables which define the parameterization of the configuration are

x_1 = wing position along fuselage
x_2 = wing dihedral angle
x_3 = wing reference area
x_4 = wing sweep angle
x_5 = wing aspect ratio
x_6 = wing leading edge extension
x_7 = wing twist angle
x_8 = fuselage camber at 16.67% of fus. length
x_9 = fuselage camber at 33.33% of fus. length
x_{10} = fuselage camber at 50.00% of fus. length
x_{11} = fuselage camber at 66.67% of fus. length
x_{12} = fuselage camber at 83.33% of fus. length
x_{13} = fuselage radius at 16.67% of fus. length
x_{14} = fuselage radius at 33.33% of fus. length
x_{15} = fuselage radius at 50.00% of fus. length
x_{16} = fuselage radius at 66.67% of fus. length
x_{17} = fuselage radius at 83.33% of fus. length

BOOM-UA is run to analyze the aerodynamic per-

formance of each design point and to compute three objective functions: the aircraft drag coefficient and the strength of the ground boom signature (using both the initial pressure rise and the perceived noise level) for each design point. The flight altitude is set at $55,000 ft$ at the cruise condition and C_L is fixed at 0.1 by allowing the angle of attack to vary during the process of a flow solution. The near-field pressure at 1.2 body lengths below the configuration was extracted on the symmetry plane. Using this signature, the ground boom signature is then computed by propagating it to the ground plane. In addition to the initial pressure rise of the signature, the overall perceived noise level is also computed for more practical designs of low-boom configurations. This measure is used because of the fact that the reduction of the initial pressure rise often leads to stronger shocks elsewhere in the wave which would result on a louder ground boom and that would not be captured by this performance measure. Based on the computed values of these objectives, Kriging approximation models are constructed and used in combination with the NSGA-II for optimization. Figure 12 shows the baseline point and the initial 232 sample points. After running NSGA-II to convergence, the CFD validation of the predicted optimal Pareto set shows that some of the points in the initial database are very close to the optimal Pareto front itself. Without loss of accuracy, the best sample point in the first design cycle can then be used as the baseline configuration for the second design cycle. However with the addition of simplified constraints for trim, longitudinal stability, and fuel volume (based on wing area, since the wing thickness is not changed), this point may turn out to be infeasible. The drag coefficient is reduced by 17.5% from 0.0112978 to 0.0093134 and the ground boom initial pressure rise is reduced by as much as 13.7% from the baseline (from 0.633 to 0.546 psf). The overall perceived noise level is reduced by about 2%. This implies that substantial reductions in the initial pressure rise do not necessarily guarantee that that perceived noise level will decrease in the same proportion. Comparing the results in figures 14 and 13, one can see that the disturbances in the near-field pressure distribution are much larger in the case of the baseline configuration. Detailed near-field pressure distributions are compared in figure 15. Due to the smaller disturbances in the near-field, this design point shows a better ground boom signature than the baseline as can be seen in figure 16.

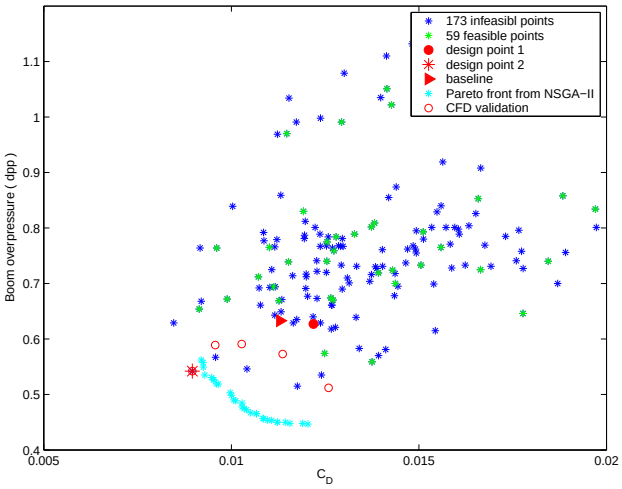

Fig. 12 1_{st} Design cycle results using Kriging-based NSGA-II.

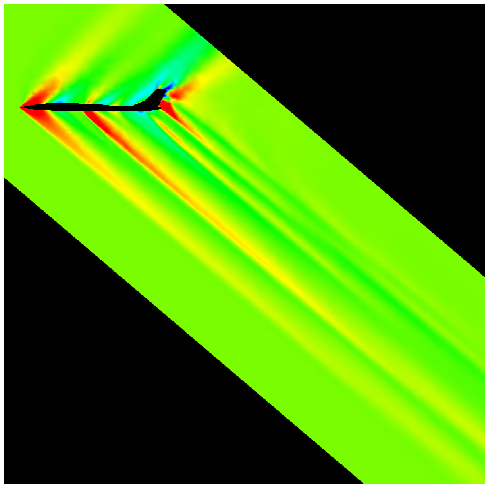

Fig. 13 Pressure plot on the symmetry plane for the baseline configuration, M=1.5

Realistic Constraints

Previous studies on the minimization of the ground signature often led to unrealistic shapes due to the lack of the consideration of reasonable problem constraints. In previous work and without the ability to change the wing reference area, the optimized shape can have a highly swept wing[4] which may cause structural instabilities and the inability to trim the configuration. The best sample point from the first cycle in this work shows similar lack of feasibility as can be seen in figure 22. The wing area has decreased significantly and the location of the wing has moved backwards. The decrease in the wing area will cause a reduction in the available fuel volume thus making the aircraft fail its range requirements. Furthermore, the increase in stall speed will cause the field length requirements to be exceeded. The change in wing position will affect the longitudinal stability since the center of pressure has now moved backwards as well. These unrealistic designs require the introduction of, at least, some basic constraints. In this study, and starting from the results from the first design cycle, two constraints are imposed: a simplified version of trim and longitudinal stability that prohibits the center of pressure from moving further aft than a specified location, and a lower limit on the wing surface area so that stall speed and fuel volume may not change significantly.

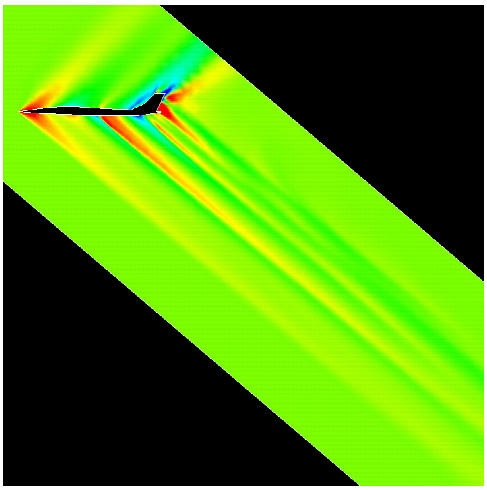

Fig. 14 Pressure plot on the symmetry plane for the best sampled configuration, M=1.5

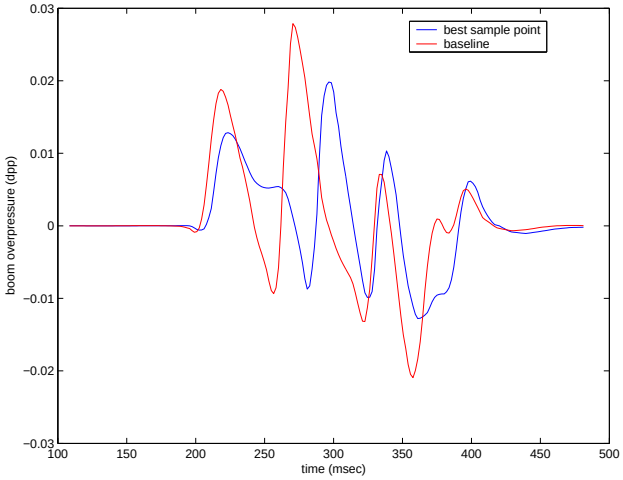

Fig. 15 Comparison of near-field pressure distributions of the best sample point (design point 2) and the baseline configuration.

Assuming that the center of gravity is located at 65% of the fuselage length (a reasonable assumption given that the aircraft has rear-mounted nacelles), the rearmost location of the center of pressure of the wing can be obtained from a simplified trim condition:

$$M_{cg} = (X_{cp_{max}} - X_{cg}) \times W - L_{T_{max}} \times (X_T - X_{cg}) = 0, \quad (11)$$

where M_{cg} is the total pitching moment about the center of gravity, $X_{cp_{max}}$ is the distance from the nose of the fuselage to the center of pressure and X_{cg} is the distance to the center of gravity. W is the total gross weight of the configuration and $L_{T_{max}}$ is the maximum lift that can be generated by the horizontal tail. The location of the center of pressure is obtained with the assumption that the wing has an elliptical load distribution in the spanwise direction and the local lift vector acts at the 40% chord location. For the initial baseline configuration, $X_{cp_{max}}$ was located at about 100 ft away from the nose of the fuselage

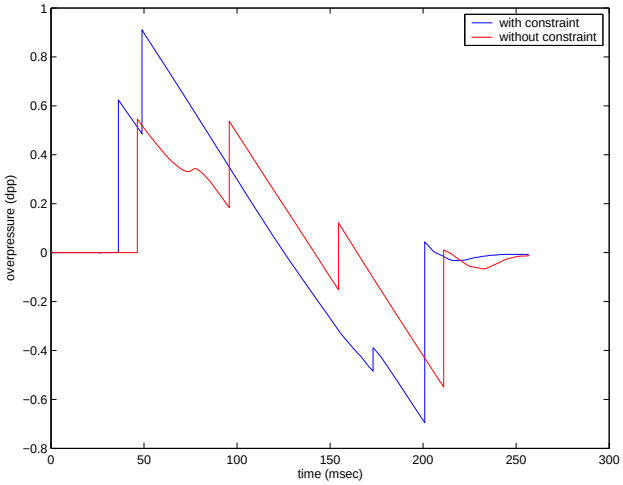

Fig. 16 Comparison of ground boom signatures between the best sample point (design point 2) and the baseline configuration.

(the fuselage is 150 ft in length.) The allowable minimum wing area is set to 79% of the wing area of the baseline configuration. With these two simplified constraints, it turns out that the best design point in the first design cycle was infeasible, and therefore it is not an appropriate choice for the baseline for the second design cycle. Instead, we select a different design point that satisfies the constraints and that also has reasonable aerodynamic performance and boom characteristics. Of the 232 initial sample points, the feasible designs are highlighted in figure 12. Among the 59 feasible points, design point 1 shows rather reasonable values of both boom loudness and drag coefficient and therefore it is chosen as the baseline configuration for the second design cycle. By choosing this point as the baseline for the second design cycle, more realistic configurations can be selected with better ground boom and aerodynamic properties. Figure 21 shows the two baseline configurations for each design cycle. For the second design cycle, the wing of the new baseline has moved forward and the wing sweep has decreased by a small amount. In the second design cycle and centered around the new baseline, another 167 sample points are chosen with a similar procedure to that used in the first design cycle. When considering the two constraints described above, about 75% of the total samples are chosen to satisfy the constraints, and another 25% of the sample points are chosen to violate the constraints slightly. Using these selections, the Kriging approximation model can have more information about the location of the constraints within the design space. Figure 17 shows the second 167 design points and the Pareto fronts for the initial pressure rise and the drag coefficient. Figure 18 shows the Pareto front for the perceived noise level and drag coefficient optimization. For both cases, Pareto fronts with constraints and without constraints are shown. In figure 17, there is not much difference between the con-

strained and unconstrained Pareto fronts, but figure 18 shows larger differences between the same two Pareto fronts. As one can expect, the Pareto front computed with the constrained version of the GA has slightly higher values of the drag coefficient, initial pressure rise and perceived noise level. For the boom initial pressure rise optimization, the reduction in the initial peak was 10.08% while the reduction in the drag coefficient was 17.38%. For the perceived noise level optimization, the reduction in noise level was much less: only about 2%. The reason for this smaller reduction in perceived noise level is that perceived noise level is usually governed by the overall shapes of the wave and not only by the initial peak of the wave, and in our work the design variables are mainly involved in changes in the wing and fuselage and they are not sufficient to reduce the 2nd peak of the wave which is affected by the rear portions of the configuration including the nacelles and empennage. Additional design changes in this portion of the configuration (which is notably the most complicated to design) can result in larger reductions in the perceived noise level and it is left for future work. A comparison of the ground boom signatures between the baseline and the boom optimized configuration is shown in figure 19. A comparison between the ground boom signatures of the baseline and the perceived noise level optimized configuration is shown in figure 20. For both of the figures, there is not much difference in the ground boom signatures The corresponding shapes that generate these signatures are shown in figures 23 and 24.

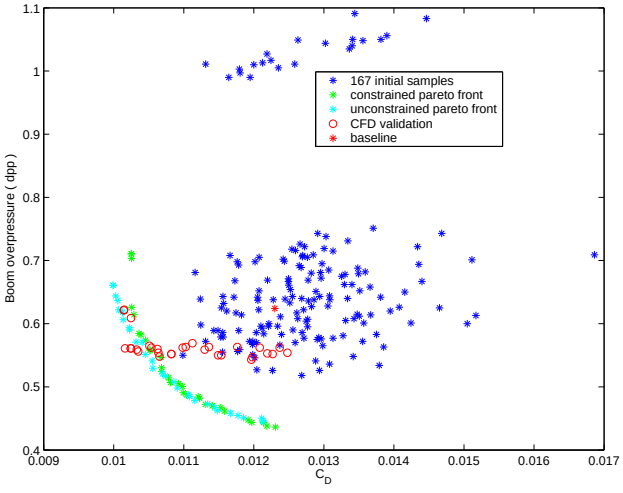

Fig. 17 2_{nd} Design Cycle Results using Kriging-Based NSGA-II for Drag Coefficient and Initial Pressure Rise.

Conclusions and Future Work

In this work, we have described a procedure based on high-fidelity analysis for the simultaneous optimization of the aerodynamic performance (coefficient of drag at fixed lift) and the loudness of complete configuration supersonic aircraft. The procedure uses the BOOM-UA environment, Kriging approximations, and a non-dominated sorting genetic algorithm to obtain optimum designs.

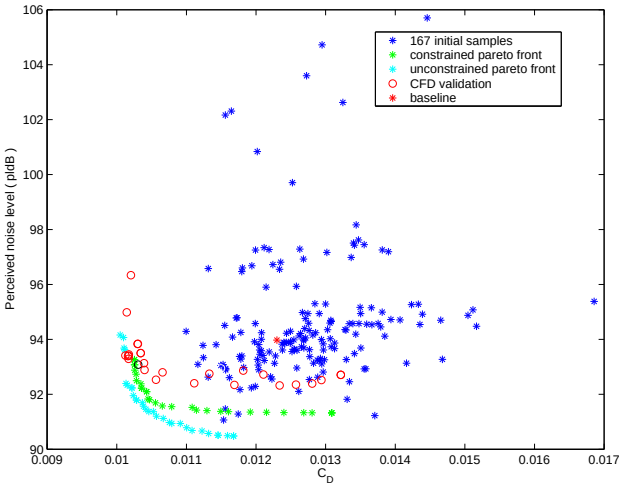

Fig. 18 2_{nd} Design Cycle Results using Kriging-Based NSGA-II for Drag Coefficient and Perceived Noise Level.

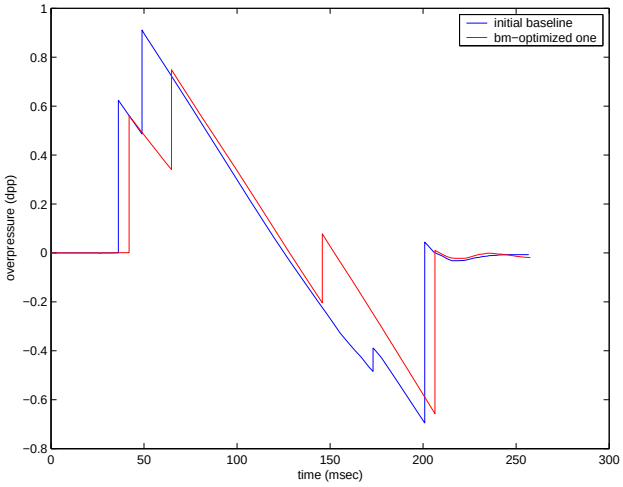

Fig. 19 Comparison of the Ground Boom Signature Between Baseline and Initial Pressure Rise Optimized Configuration During the Second Design Cycle.

A configuration that had been previously optimized for aerodynamic performance was chosen as the baseline for the 1st design cycle of a multi-objective optimization. The result of this design cycle is a configuration with significantly less drag and lower sonic boom loudness. However, this unconstrained design did not meet the stability, range, and take-off and landing requirements we had setup. For this reasons, a sub-optimal design which satisfied all constraints and had reasonable aerodynamic performance was chosen as the baseline for the second design cycle. The Kriging-based genetic algorithm procedure gives shapes which are optimized for both the initial peak and perceived noised level of the signature along with minimum drag.

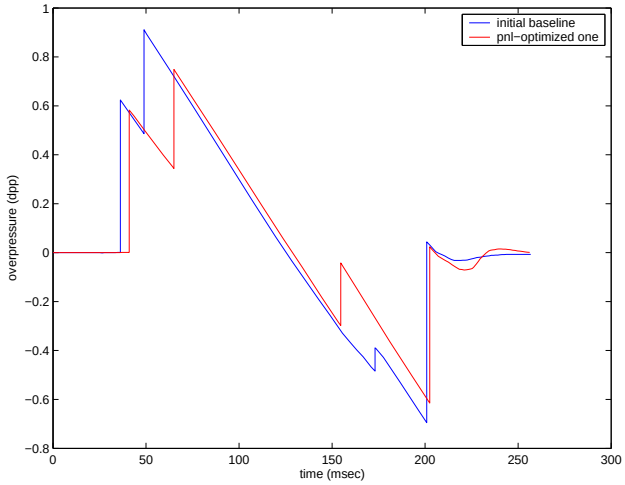

Fig. 20 Comparison of the Ground Boom Signature Between Baseline and boom initial peak optimized configuration in the second design cycle

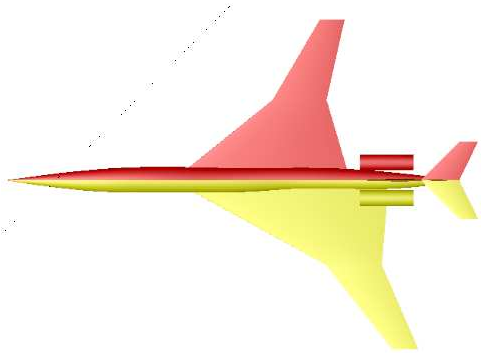

Fig. 21 Baseline configurations for the first design cycle (bottom) and for the second design cycle (top)

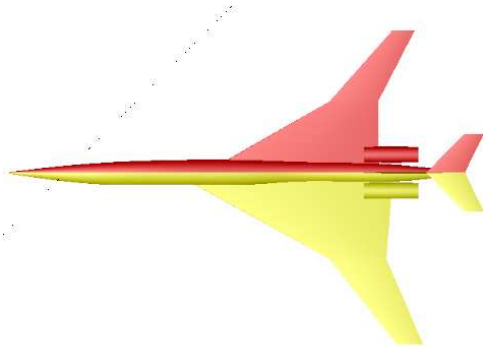

Fig. 22 Configuration for the best design point and the baseline

The differences between these shapes produced are small because of the fact that the parameterization of the design does not include changes in the rear part of the configuration which may reduce the pressure disturbance in the near-field and result in smaller second peaks in the ground boom signatures. The appropriate selection of the design variables to reduce the 2nd peak of the ground boom signature will be considered in future work.

Fig. 23 Configuration optimized for minimum boom

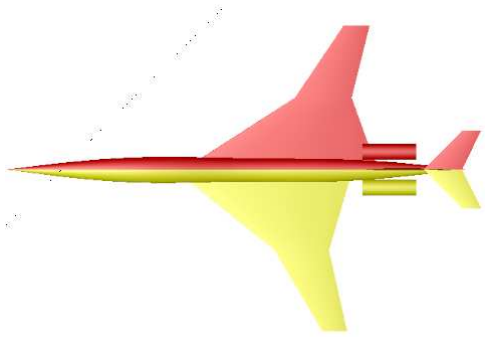

Fig. 24 Configuration optimized for minimum pnl

This study, however, demonstrates the feasibility of using high-fidelity modeling for design in multi-objective situations. Even though the cost of a single analysis is relatively large, solution-adaptive methods with meshes with over 5 million nodes (to appropriately resolve the physical phenomena) can be of practical use today.

Future work will concentrate in further refinements to the approximation techniques in order to improve the quality of the fits for highly discontinuous functions such as the boom loudness. In addition, we intend to include mixtures of high- and low-fidelity models in order to improve our ability to achieve optimal designs in high-dimensional spaces.

Acknowledgments

This work has been carried out under the support of the NASA Langley Research Center, under contract NAG-1-03046. We gratefully acknowledge the support of our point of contact, Dr. Peter Coen, in supplying us with the geometry and experimental data necessary to complete the validation portion of this study. We also appreciate the invaluable help of Dr. Edwin van der Weide for allowing us to use the AirplanePlus flow solver for this study and of Mr. Ki-Hwan Lee for creating a parallel version of the NSGA-II optimizer.

References

[1]National Research Council, High Speed Research Aeronautics and Space Engineering Board *U.S. Supersonic Commercial Aircraft : Assessing NASA's High Speed Research Program* , National Academy Press, Washington, D.C., 1997.

[2]National Research Council, High Speed Research Aeronautics and Space Engineering Board *Commercial Supersonic Technology : The Way Ahead* , National Academy Press, Washington, D.C., 2002.

[3]S. Choi, J. J. Alonso and E. Weide. "Numerical and Mesh Resolution Requirements for Accurate Sonic Boom Prediction of Complete Aircraft Configurations". *AIAA Paper 2004-1060* 42nd AIAA Aerospace Sciences Meeting and Exhibit, Reno, Neveda, Jan 2004.

[4]H. Chung and J. J. Alonso "Hyoung S. Chung, Seongim Choi, Juan J. Alonso," *21st Applied Aerodynamics Conference*, AIAA 2003-3791, Orlando, FL, June 2003.

[5]H. S. Chung. *Multidisciplinary Design Optimizationof Supersonic Business Jets Using Approximation Model-Based Genetic Algorithms.* PhD thesis, Stanford University, Stanford, CA 94305, 2004. To be published.

[6]H. Chung and J. J. Alonso "Design of a Low-Boom Supersonic Business Jet Using Cokriging Approximation Models," *9th AIAA/ISSMO Symposium on Multidisciplinary Analysis and Optimization*, AIAA 2002-5598, Atlanta, GA, September 2002.

[7]M. Chan, "Supersonic Aircraft Optimization for Minimizing Drag and Sonic Boom," PhD thesis, Stanford University, Stanford, CA 94305, 2003.

[8]D. Aronstein and K. Schueler "Conceptual Design of a Sonic Boom Constrained Supersonic Business Aircraft" *42nd AIAA Aerospace Sciences Meeting and Exhibit*, AIAA-2004-697, Reno, NV, January, 2004.

[9]Nadarajah, S. K., Kim, S., Jameson, A., and Alonso, J. J. "Sonic Boom Reduction Using an Adjoint Method for Supersonic Transport Aircraft Configuration," *Symposium Transsonicum IV, International Union of Theoretical and Applied Mechanics*, September 2-6, 2002, DLR Gottingen, Germany

[10]F. J. Wilcox. *Business Jet Sonic Boom Test - Unitary Plan Wind Tunnel Test 1870.* NASA Langley Research Center, February 2000.

[11]J. Reuther and J. J. Alonso and A. Jameson and M. Rimlinger and D. Saunders "Constrained Multipoint Aerodynamic Shape Optimization Using an Adjoint Formulation and Parallel Computers: Part I," *Journal of Aircraft, 36:51-60.* 1999

[12]J. Reuther and J. J. Alonso and A. Jameson and M. Rimlinger and D. Saunders "Constrained Multipoint Aerodynamic Shape Optimization Using an Adjoint Formulation and Parallel Computers: Part II," *Journal of Aircraft, 36:61-74.* 1999

[13]A. Jameson "Aerodynamic Design via Control Theory," *Journal of Scientific Computing, 3:233-260* 1988

[14]Hamies, R. and Follen, G. "Computational Analysis Programming Interface," *Proceedings of the 6th International Conference on Numerical AlonGrid Generation in Computational Field Simulations*, Greenwich, 1998

[15]R. Lohner Finite-element methods in CFD: Grid generation, adaptivity and parallelization *In von karman Institute Series, AGARD Pub.R-787* 1992

[16]G. Warren, W. K. Anderson, J. L. Thomas and S. L. Krist Grid Convergence for Adaptive Methods *AIAA paper 91-1592*, June 1991

[17]J. J. Alonso, J. R. R. A. Martins, J. J. Reuther, R. Haimes, and C. A. Crawford "High-Fidelity Aero-Structural Design Using a Parametric CAD-Based Model," *16th AIAA Computational Fluid Dynamics Conference*, AIAA 2003-3429, Orlando, FL., 2003.

[18]J. J. Alonso, I. M. Kroo and A. Jameson. Advanced Algorithms for Design and Optimization of Quiet Supersonic Platforms. *AIAA Paper 02-0114*, 40th AIAA Aerospace Sciences Meeting and Exhibit, January 2002, Reno, NV.

[19]L. Fornasier, H. Rieger, U. Tremel, E. Van der Weide. *Time Dependent Aeroelastic Simulation of Rapid Maneuvering Aircra ft. AIAA Paper 02-0949*, 40th AIAA Aerospace Sciences Meeting and Exhibit, January 2002, Reno, NV.

[20]T. J. Baker. Mesh Adaptation Strategies for Problems in Fluid Dynamics. *Finite Elements in Analysis and Design*, Vol. 25, 1997, pp. 243-273.

[21]M. A. Park. Adjoint-Based, Three-Dimensional Error Prediction and Grid Adaptation. *32nd Fluid Dynamics Conference*, June 24-27, 2002, St. Louis, MO

[22]R. Lohner. Generation of Unstructured Grids Suitable for RANS Calculations *AIAA Paper 99-0662*, 1999

[23]D. J. Mavriplis. Unstructured Mesh Generation and Adaptivity *ICASE 95-26*

[24]J. Peraire, M. Mahdati, K. Morgan and O. C. Zienkienwicz Adaptive Remeshing for Compressible Flow Computation *Journal of Computational physics, 72:449-466* October, 1987

[25]A. Jameson, T. J. Baker and N. P. Weatherill. Calculation of Inviscid Transonic Flow over a Complete Aircraft. *AIAA Paper 86-0103*, 24th Aerosapce Sciences Meeting, January 6-9, 1986, Reno, Nevada

[26]J. R. Koehler and A. B. Owen "Computer Experiments," *Handbook of Statistics Vol. 13*, pp. 261-308, Elsevier Science, New York, eds. S. Ghosh and C. R. Rao

[27]Timothy W. Simpson, Timothy M. Mauery, John J. Korte and Farrokh Mistree "Comparison of Response Surface and Kriging Models in the Multidisciplinary Design of an Aerospike Nozzle," *7th AIAA/USAF/NASA/ISSMO Symposium on Multidisciplinary Analysis and Optimization*, St. Louis, Missouri, AIAA 98-4755, September 1998

[28]Anthony A. Giunta and Layne T. Watson "A Comparison of Approximation Modeling Techniques: Polynomial Versus Interpolating Models," *7th AIAA/USAF/NASA/ISSMO Symposium on Multidisciplinary Analysis and Optimization* , St. Louis, Missouri, AIAA 98-4758, September 1998.

[29]Wallace D. Hayes, Rudolph C. Haefeli and H.E.Djlsrud "Sonic Boom Propagation in a Stratified Atmosphere, with computer Program" *NASA CR-1299*,1969

[30]Thomas,Charles L. "Extrapolation of Wind-Tunnel Sonic Boom Signatures without Use of a Whitham F-function" *NASA SP-255, pp.205-217*,1970

[31]Kenneth J. Plotkin "PCBoom3 Sonic Boom Prediction Model-Version 1.0e," *Wyle Research Report WR 95-22E*, October. 1998.

[32] *Centaur System Users' Manual*, *http://www.centaursoft.com*

[33]Jaroslaw Sobieszczanski-Sobieski and Raphael T. Haftka "Multidisciplinary Aerospace Design Optimization: Survey of Recent Developments," *34th AIAA Aerospace Sciences Meeting and Exhibit* , Reno, Nevada, AIAA 96-0711, January 1996.

[34]Thomas A. Zang and Lawrence L. Green. "Multidisciplinary Design Optimization Technique: Implications and Opportunities for Fluid Dynamics" *30th AIAA Fluid Dynamics Conference*, Norfolk, Virginia, AIAA 99-3798, June 1999

[35]Resit Unal, Roger A. Lepsch, Jr. and Mark L. McMillin "Response Surface Model Building and Multidisciplinary Optimization Using Overdetermined D-Optimal Designs," *7th AIAA/USAF/NASA/ISSMO Symposium on Multidisciplinary Analysis and Optimization*, AIAA 98-4759, September 1998

[36]J. Martin, J. J. Alonso and J. Reuther "High-Fidelity Aero-Structural Design Optimization of a Supersonic Business Jet," *43rd AIAA/ASME/ASCE/AHS/ASC Structures, Structural Dynamics, and Materials Conference*, AIAA 2002-1483, Denver, CO, April 2002.

[37]J. Martin and J. J. Alonso "Complete Configuration Aero-Structural Optimization Using a Coupled Sensitivity Analysis Method," *9th AIAA/ISSMO Symposium on Multidisciplinary Analysis and Optimization*, AIAA 2002-5402 Atlanta, GA, September 2002.

[38]J. Sacks, W. J. Welch, T. J. Michell, and H. P. Wynn "Design and Analysis of Computer Experiments," *Statistical Science Vol 4. No.4*, pp. 409-453, 1989

[39]N. Srinivas and K. Deb, "Multiobjective Optimization Using Nondominated Sorting in Genetic Algorithm," *Evolutionary Computation*,2(3):221-248, 1995.

[40]N. Marco and S. Lanteri, "Parallel Genetic Algorithms applied to Optimum Shape Design in Aeronautics," *Euro-Par'97 parallel Processing*, pages 856-863, Passau (Germany), Springer Verlag, 1997

[41]C. A. Coello Coello and G. T. Pulido "A Micro-Genetic Algorithms for Multiobjective Optimization," *Proceedings of the Genetic and Evolutionary Computation Conference (GECCO'2001)* , 2001.

[42]K. Krishnakumar "Micro-genetic algorithms for stationary and non-stationary function optimization," *SPIE Proceedings : Intelligent Control and Adaptive Systems, pages 289-296*, 1989.

[43]D. L. Carroll "Fortran Genetic Algorithm Driver," *http://cuaerospace.com/carroll/ga.html*, 2001

[44]J. J. Alonso, I. M. Kroo and A. Jameson Proceedings of the DARPA QSP Technical Exchange Meeting 5. December 2001.